Post-Exfoliation Functionalisation of Metal-Organic Framework Nanosheets via Click Chemistry

Supplementary Information

Joshua Nicks, and Jonathan A. Foster*

University of Sheffield, Department of Chemistry, Sheffield, S3 7HF, UK

Table of Contents

S1. General Details

S1.1. Materials

Commercial solvents, reagents and spectroscopic grade deuterated solvents were used as purchased without further purification, as listed: copper acetate monohydrate (98+%, Alfa Aesar), 2-aminoterephthalic acid (99%, Alfa Aesar), t-butyl nitrate (≥90%, Sigma-Aldrich), trimethylsilyl azide (94%, Alfa Aesar), tetrakis(acetonitrile)copper(I) hexafluorophosphate (97%, Sigma-Aldrich), propiolic acid (98+%, Alfa Aesar), 3-butyn-1-ol (97%, Fluorochem), 3-dimethylamino-1-propyne (97%, Sigma-Aldrich), 1-ethynylpyrene (98+%, Alfa Aesar), acetonitrile (≥99%, Fisher), dimethylformamide (≥99%, Fischer), diethyl ether (≥99.8%, Sigma-Aldrich), tetrahydrofuran (≥99%, VWR), nitrobenzene (≥99.0%, Merck), dimethyl sulfoxide-d_6 (99.5 atom % D, Sigma-Aldrich), deuterium chloride solution (35 wt. % in D2O, ⩾99 atom % D, Sigma-Aldrich).

S1.2. Details of Analytical Procedures

Elemental analysis was performed by the microanalytical service at the Department of Chemistry, University of Sheffield using a Vario MICRO Cube in an atmosphere of pure O_2. Elemental CHN contents are determined to a tolerance of ± 0.5 % for organometallics.

FT-IR spectra were recorded using a Perkin Elmer Spectrum 100 FT-IR spectrophotometer, equipped with a SenseIR diamond ATR module. Samples were analysed without further preparation, and spectra were obtained in reflectance mode between 4000 – 600 cm^{-1}, using 12 scans with a spectral resolution of 1 cm^{-1}.

NMR spectra were recorded at 300 K using a Bruker Avance III HD 400 spectrometer equipped with a standard geometry 5mm BBFO probe with a single z-gradient at 400 MHz (^1H), or using a Bruker AV 400 spectrometer with a 5mm solution state probe at 400 MHz (^1H). Supramolecular frameworks were digested prior to submission, using DCl (5 µL) and DMSO-d_6 (1 mL). NMR spectra were processed using MestreNova. Mass spectra were recorded directly from NMR solutions using an Agilent 6530 QTOF LC-MS in negative ionisation mode.

UV-visible absorption (UV-Vis) spectra were obtained using a Varian Cary 50 Bio spectrophotometer using standard 1 cm width quartz cells and Perkin Elmer Spectrum One

software. Spectral data was formatted using Microsoft Excel. Emission spectra were recorded using a Horiba Jobin Yvon Fluoromax-4-Spectrofluorimeter and were corrected using correction files included within the FluorEssence™ software. Data was formatted using Origin Pro.

Powder X-ray diffraction (XRD) data were collected using a Bruker-AXS D8 diffractometer using Cu K_α (λ=1.5418 Å) radiation and a LynxEye position sensitive detector in Bragg Brentano parafocussing geometry using a packed glass capillary or a flat silicon plate.

Thermogravimetric analyses (TGA) were performed using a Perkin-Elmer Pyris 1 instrument. Approximately 4 mg of sample was weighed into a ceramic pan, held under nitrogen flow of 20 cm^3 min^{-1} at 25 °C for 10 minutes to purge the sample and allow for equilibration, then ramped to varying end temperatures (see individual traces for details) at 1 °C min^{-1}. The samples were then held at the final temperature for 10 minutes.

Dynamic light scattering (DLS) data were collected using a Malvern Zetasizer Nano Series particle size analyser, using a He-Ne laser at 633 nm, operating in backscatter mode (173 °). Samples were equilibrated at 298 K for 60 s prior to analysis. Zeta potential data were collected using the same instrument in zeta potential mode, using disposable polycarbonate capillary electrophoresis cells and according to the Smoluchowski method. Contact angle measurements were obtained using a Ramé-Hart Goniometer.

Atomic force microscopy (AFM) images were recorded using a Bruker Multimode 5 Atomic Force Microscope, operating in soft-tapping mode in air under standard ambient temperature and pressure, fitted with Bruker OTESPA-R3 silicon cantilevers operated with a drive amplitude of ~18.70 mV and resonance frequency of ~236 kHz. Samples were prepared by drop-casting 10 µL drops of suspension onto the centre of freshly cleaved mica sheets heated to 100 °C on a hot plate. These sheets were stuck to stainless steel, magnetic Agar scanning probe microscopy specimen discs. Images were processed using Gwyddion software.

Scanning electron microscopy (SEM) samples were prepared by loading powdered samples onto carbon sticky tabs placed on aluminium SEM sample stubs, coated with approximately 20 nm gold using an Edwards S150B sputter coater and loaded into a TESCAN VEGA3 LMU SEM, operated at 15 keV. Images were collected at 10,000x magnification using the secondary electron detector.

S2. Preparation and Characterisation of Cu(N_3-BDC)(DMF) Layered MOF

S2.1. Details of Preparation

An attempt was made to synthesise the Cu(N_3-BDC)(DMF) in an analogous fashion to our previously published for Cu(NH_2-BDC)(DMF) using 2-azidoterephthalic acid, synthesised according to a previously published procedure by Wöll *et al.* The ^{1}H NMR spectrum of this linker is shown below in figure S1. This procedure afforded only a black amorphous solid under both solvothermal conditions and reaction at room temperature.

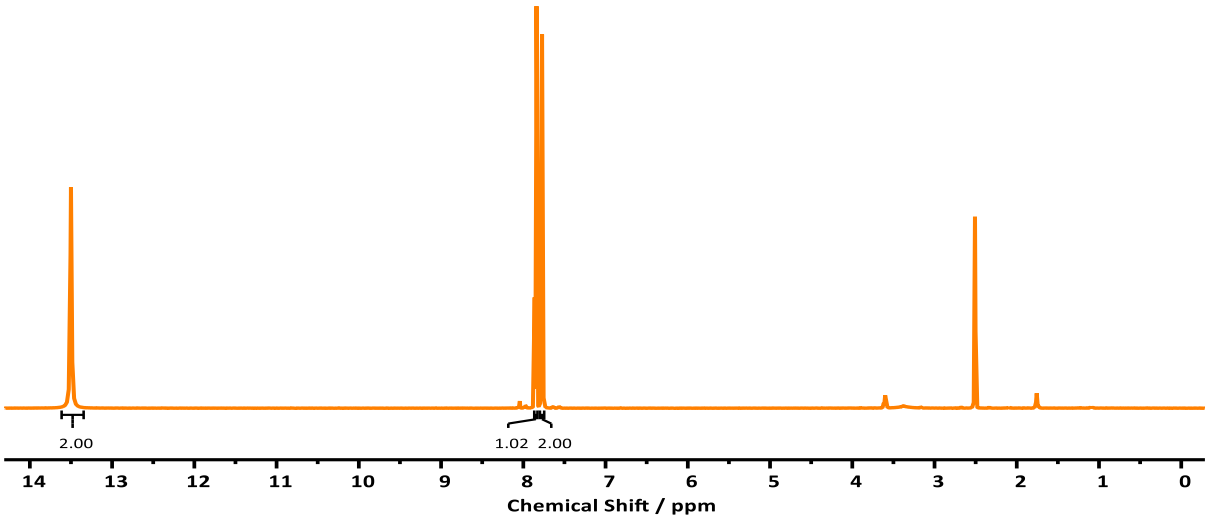

Figure S1. The ^{1}H NMR spectrum of 2-azidoterephthalic acid prepared from 2-aminoterephthalic acid.

Table S1. A table of the equivalents of t-butyl nitrite (*t*-BuONO) and azidotrimethylsilane (TMS-N_3) used to obtain varying degrees of conversion from the amino- layered MOF to the azido- layered MOF, Cu(N_3-BDC)(DMF).

***t*-BuONO Equivalents**	**TMS-N_3 Equivalents**	**Conversion / %**
0.0	0.0	0
2.6	2.4	21
4.5	4.0	52
7.9	7.1	81
11.0	9.5	100

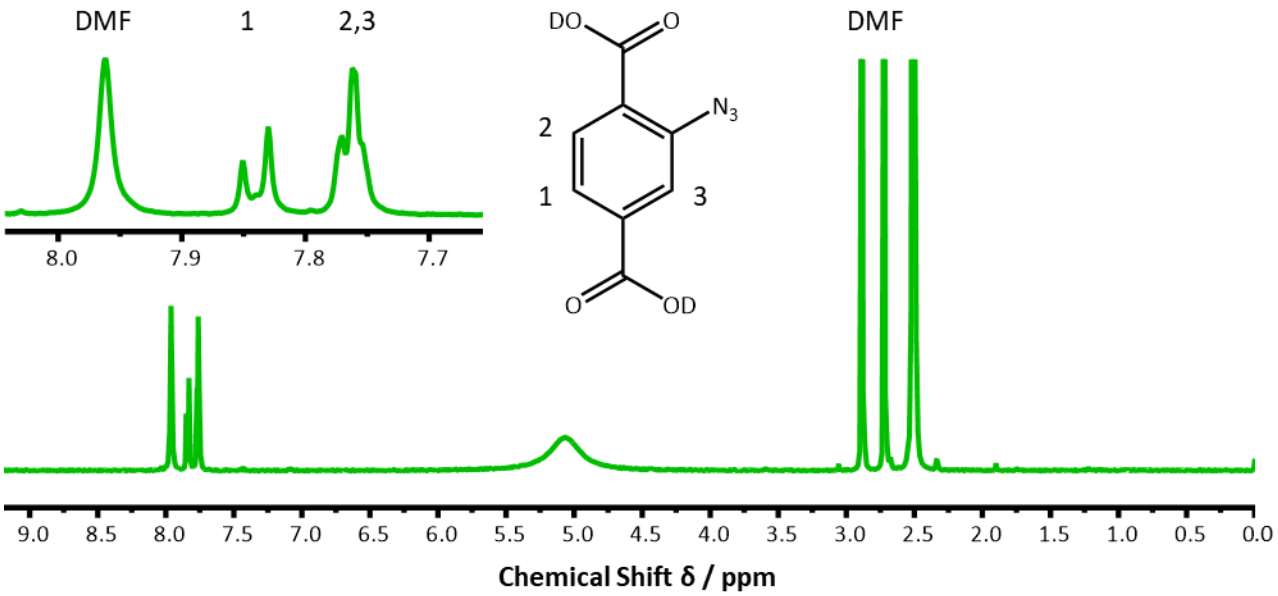

Figure S2. Annotated ^{1}H NMR spectrum of digested Cu(N_3-BDC)(DMF).

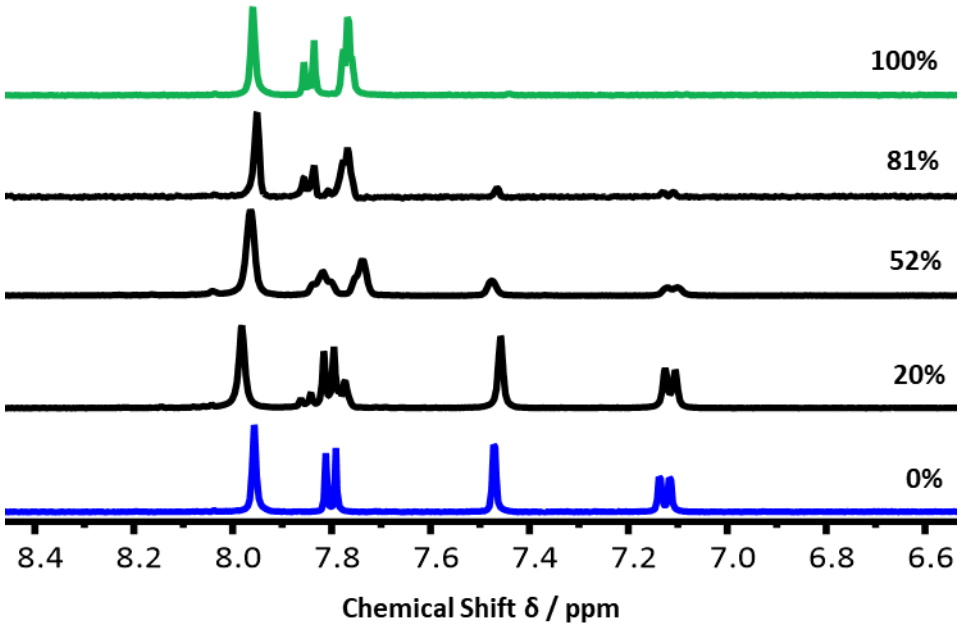

Figure S3. Stack plot of digested ^{1}H NMR spectra showing the conversion of Cu(ABDC)(DMF) into Cu(N_3-BDC)(DMF) with increasing equivalents of *t*-BuONO and TMS-N_3. Slight discrepancies in chemical shifts are a result of minor changes in DCl concentration.

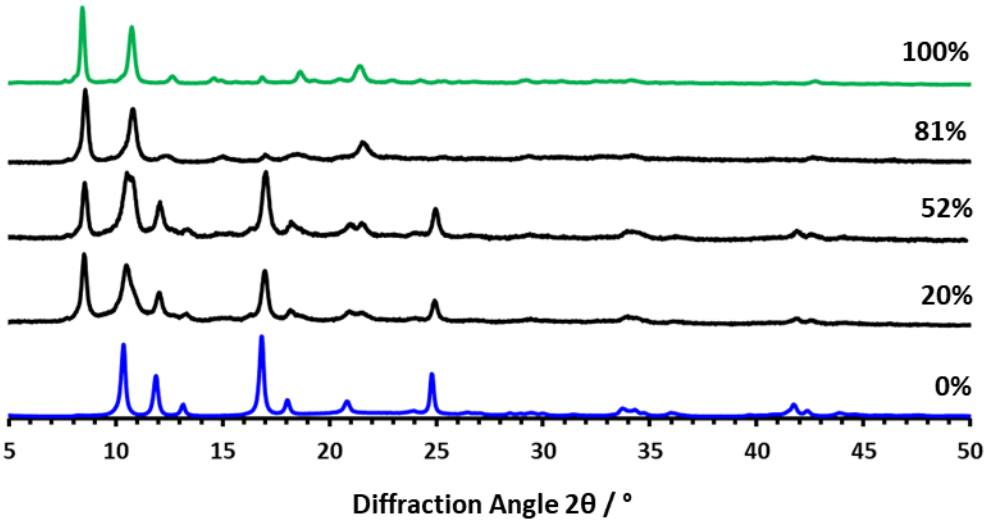

Figure S4. Stack plot of XRD powder patterns (recorded in flat plate stage), showing the conversion of Cu(ABDC)(DMF) into Cu(N_3-BDC)(DMF).

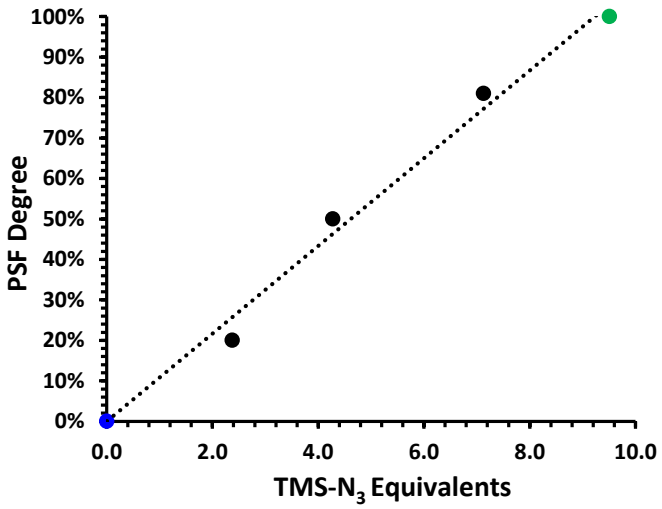

Figure S5. Plot of the values from table 1, demonstrating the tunable nature of the azidification process.

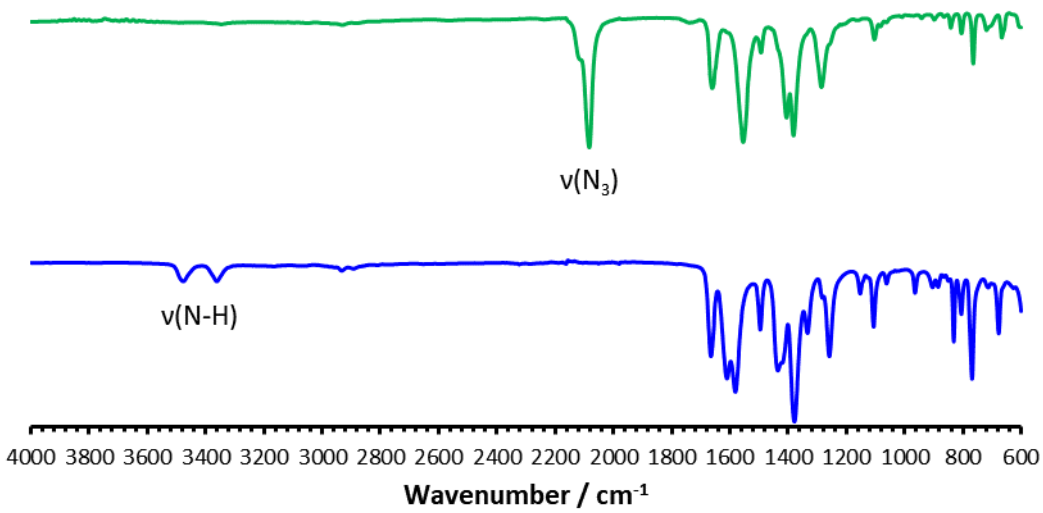

Figure S6. A comparison between the FT-IR spectra of Cu(ABDC)(DMF) (blue) and Cu(N_3-BDC)(DMF) (green), with the respective characteristic ν(N-H) and ν(N_3) peaks indicated.

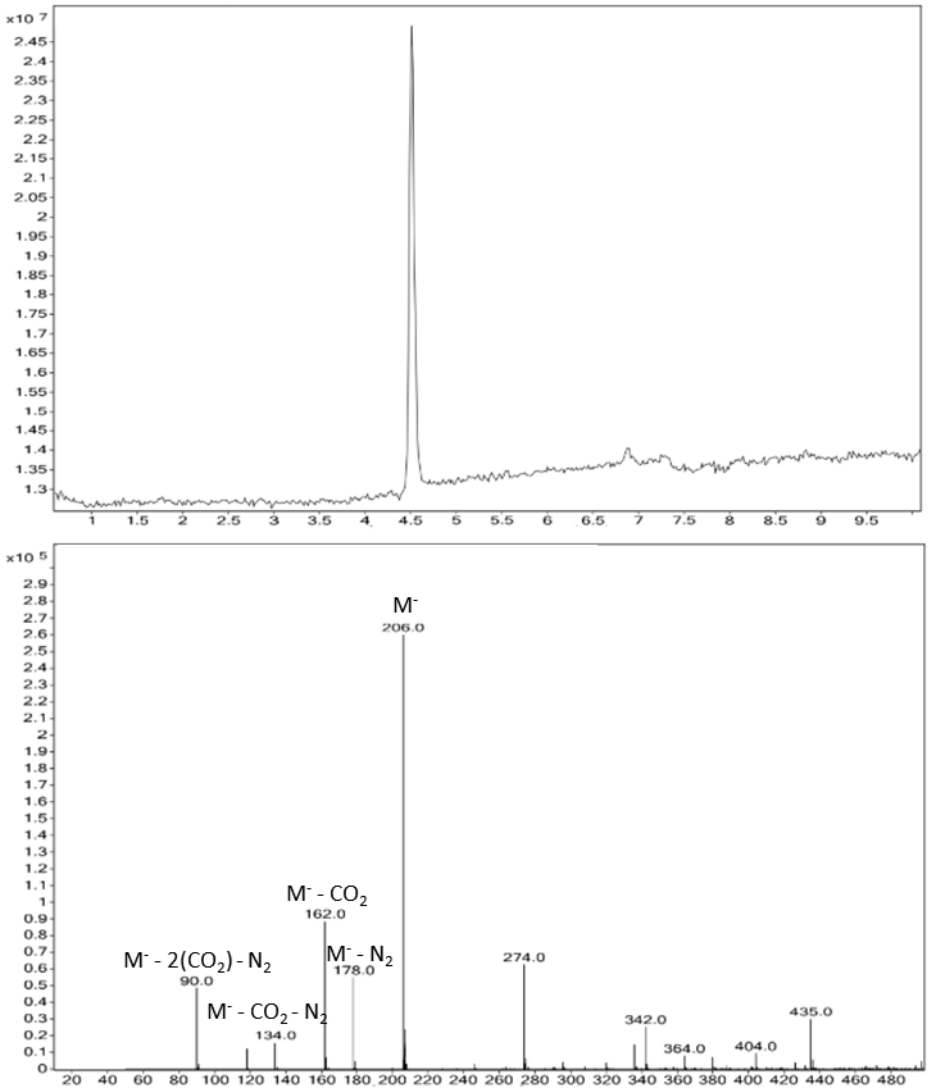

Figure S7. Assigned LC chromatograph and NEG-ESI mass spectrum of digested Cu(N_3-BDC)(DMF).

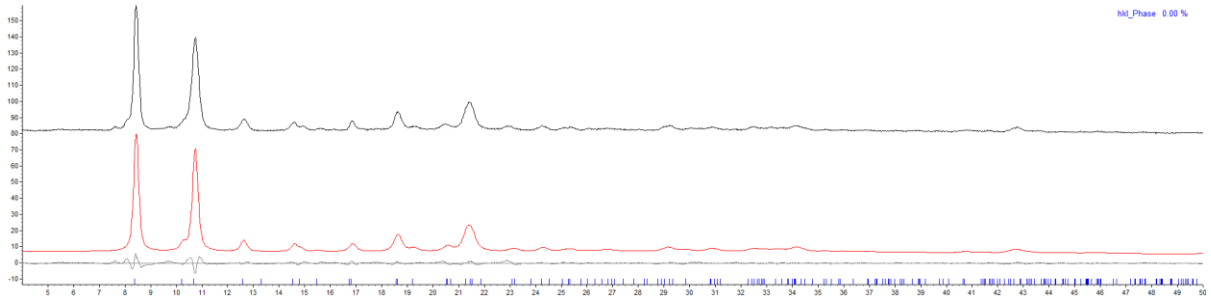

Figure S8. Fitted Pawley refinement of the Cu(N_3-BDC)(DMF) XRD pattern to the unit cell with dimensions outlined in table S2.

Table S2. The unit cell parameters obtained from Pawley refinement of the XRD pattern obtained from Cu(N_3-BDC)(DMF), compared to the unit cell parameters of MOF-46 (Zn analogue of Cu(NH_2-BDC)(DMF).[2]

MOF	Crystal System	Space Group	a / Å	b / Å	c / Å	β / °	Cell Vol. / Å^3	R_{wp}	R_{exp}
MOF-46	Monoclinic	C2/m	11.2043(9)	15.0516(12)	8.0275(7)	111.7060(10)	1257.79(18)	-	-
Cu(N_3-BDC)(DMF)	Monoclinic	C2	13.41769)	17.1225	8.3632	100.3478	1890.14	5.269	1.831

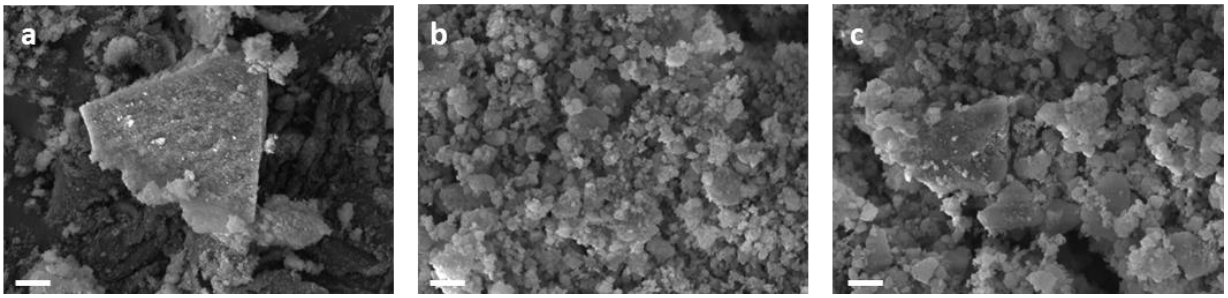

Figure S9. SEM images of **a)** Cu(ABDC)(DMF), and **b)** and **c)** Cu(N_3-BDC)(DMF). Inset scale bars represent 5 µm.

S3. Exfoliation and Characterisation of Cu(N_3-BDC)(DMF) MONs

S3.1. Exfoliation of Cu(N_3-BDC)(DMF)

Liquid-assisted ultrasonic exfoliations were carried out by suspension of 5 mg of MOF in 6 mL of acetonitrile inside a 10 mL reaction vial. The sample was mixed in a vortex mixer for 30 seconds to disperse the sediment. The samples were sonicated using a Fisherbrand Elmasonic P 30H ultrasonic bath (2.75 L, 380/350 W, UNSPSC 42281712) filled with water. Samples were sonicated for 12 hours at a frequency of 80 kHz with 100% power and the temperature was thermostatically maintained at 16-20°C using a steel cooling coil. Sonication was applied using a sweep mode and samples were rotated through the water using an overhead stirrer to minimise variation due to ultrasound "hot-spots". Suspensions of nanosheets were obtained by centrifugation at 362 xg (1500 rpm) for 1 hour, followed by removal of the suspension from the isolated bulk powder.

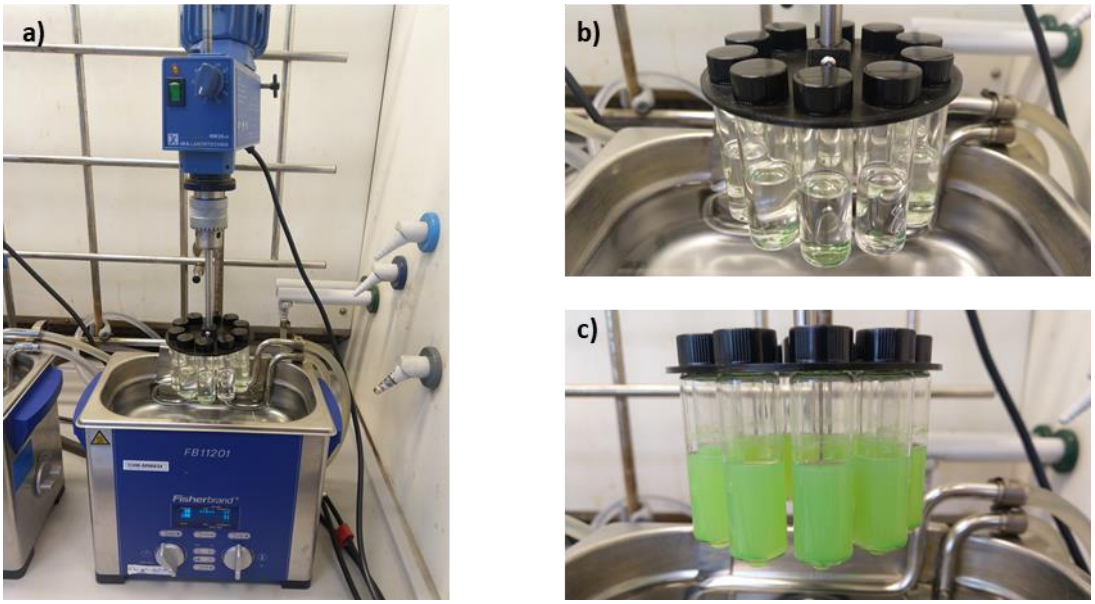

Figure S10. a) The setup used for liquid exfoliation of the Cu(N_3-BDC)(DMF) framework, **b)** and **c)** images of the samples pre- and post-exfoliation respectively.

S3.2. Characterisation of Cu(N_3-BDC) Nanosheets

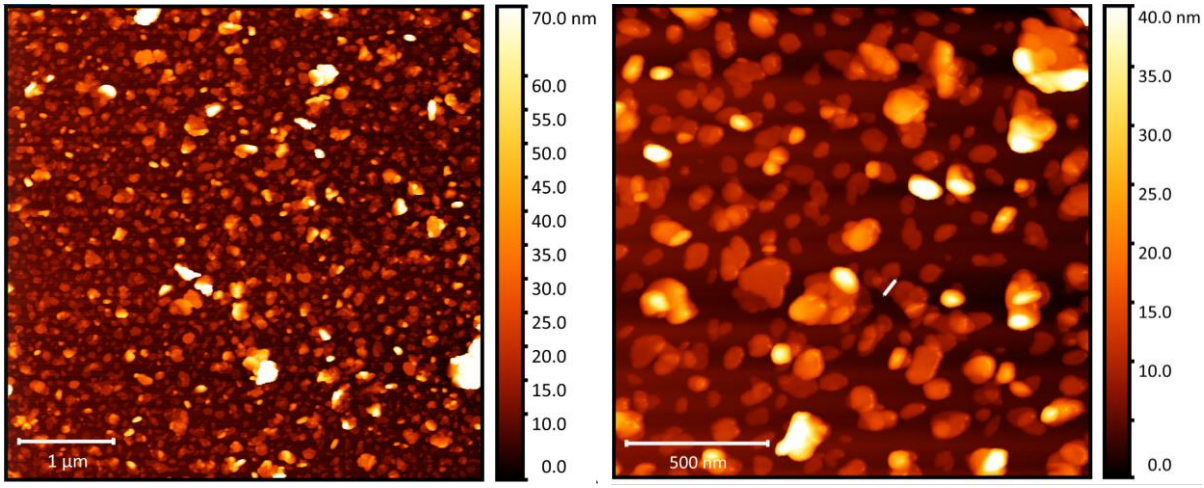

Figure S11. AFM images of the Cu(N_3-BDC) MONs obtained from ultrasonic exfoliation of the layered Cu(N_3-BDC)(DMF) MOF.

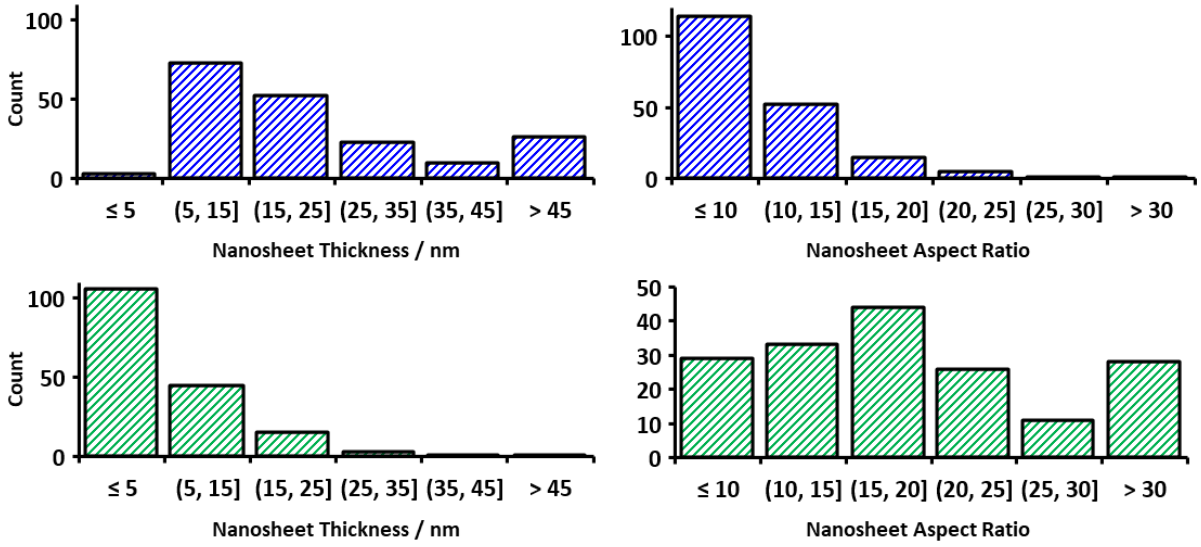

Figure S12. Size distribution histograms of both Cu(ABDC) and Cu(N_3-BDC) MONs, showing both nanosheet thickness and aspect ratio data.

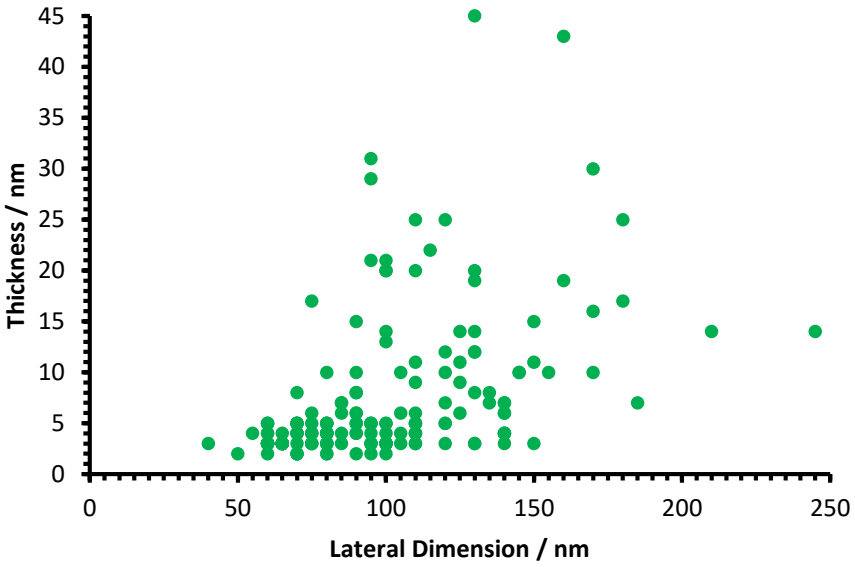

Figure S13. Size distribution scatter plot of Cu(N_3-BDC) MONs.

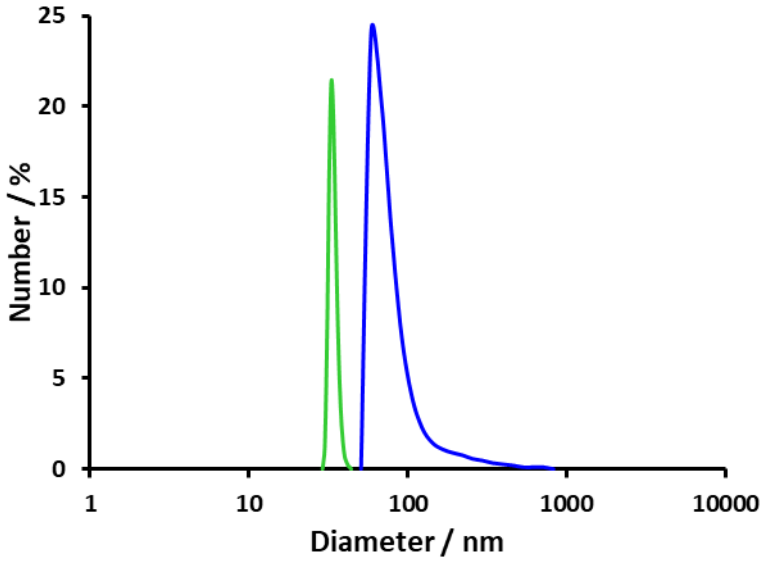

Figure S14. DLS plots of Cu(ABDC) (blue) and Cu(N_3-BDC) (green) nanosheets.

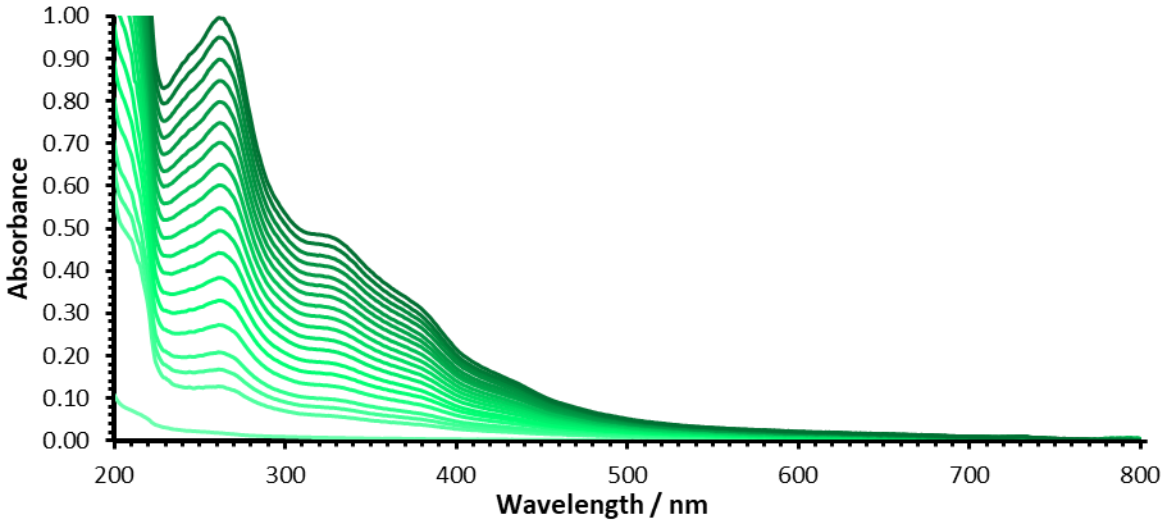

Figure S15. A series of UV-Vis spectra recorded for known concentrations of Cu(N_3-BDC) MONs used to calculate the extinction coefficient of the system.

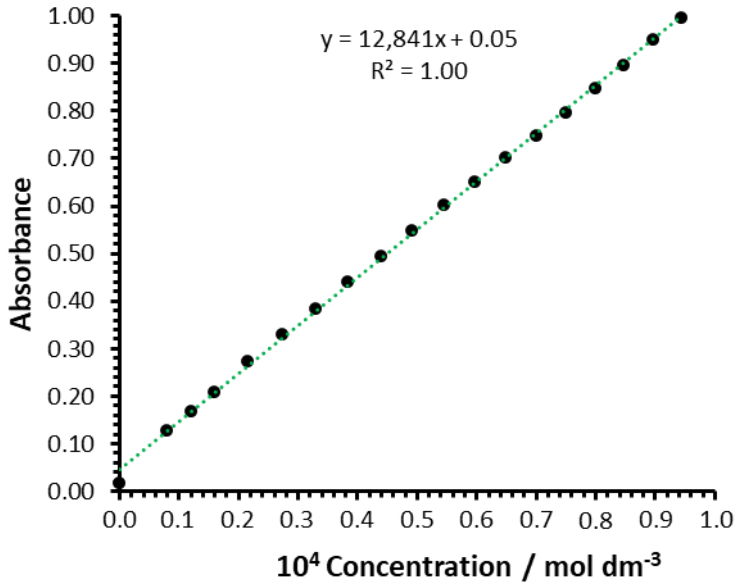

Figure S16. Plot used to calculate the extinction coefficient of the band at λ=261 nm, giving a value of 12,841 dm^3 mol^{-1} cm^{-1}.

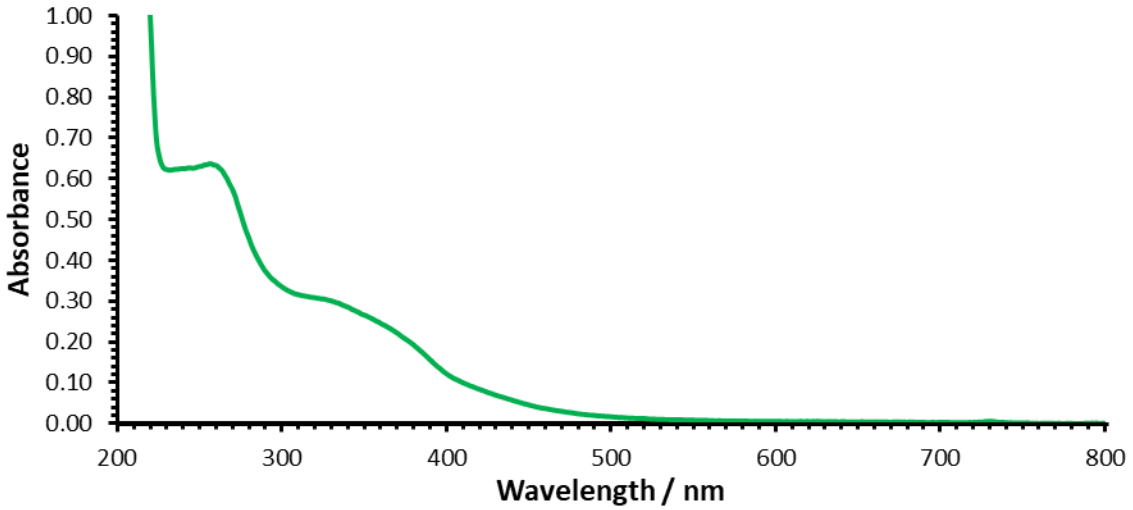

Figure S17. UV-Vis spectrum of the as exfoliated Cu(N_3-BDC) nanosheets, following centrifugation at 1500 rpm for 1 hour and dilution by a factor of 100.

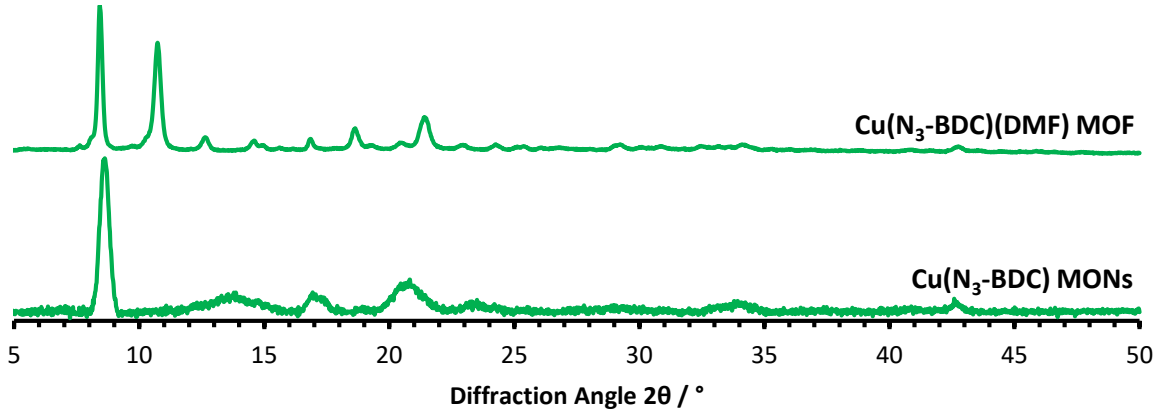

Figure S18. XRD pattern of Cu(N_3-BDC) nanosheets and Cu(N_3-BDC) layered MOF desolvated by repeated stirring in acetonitrile.

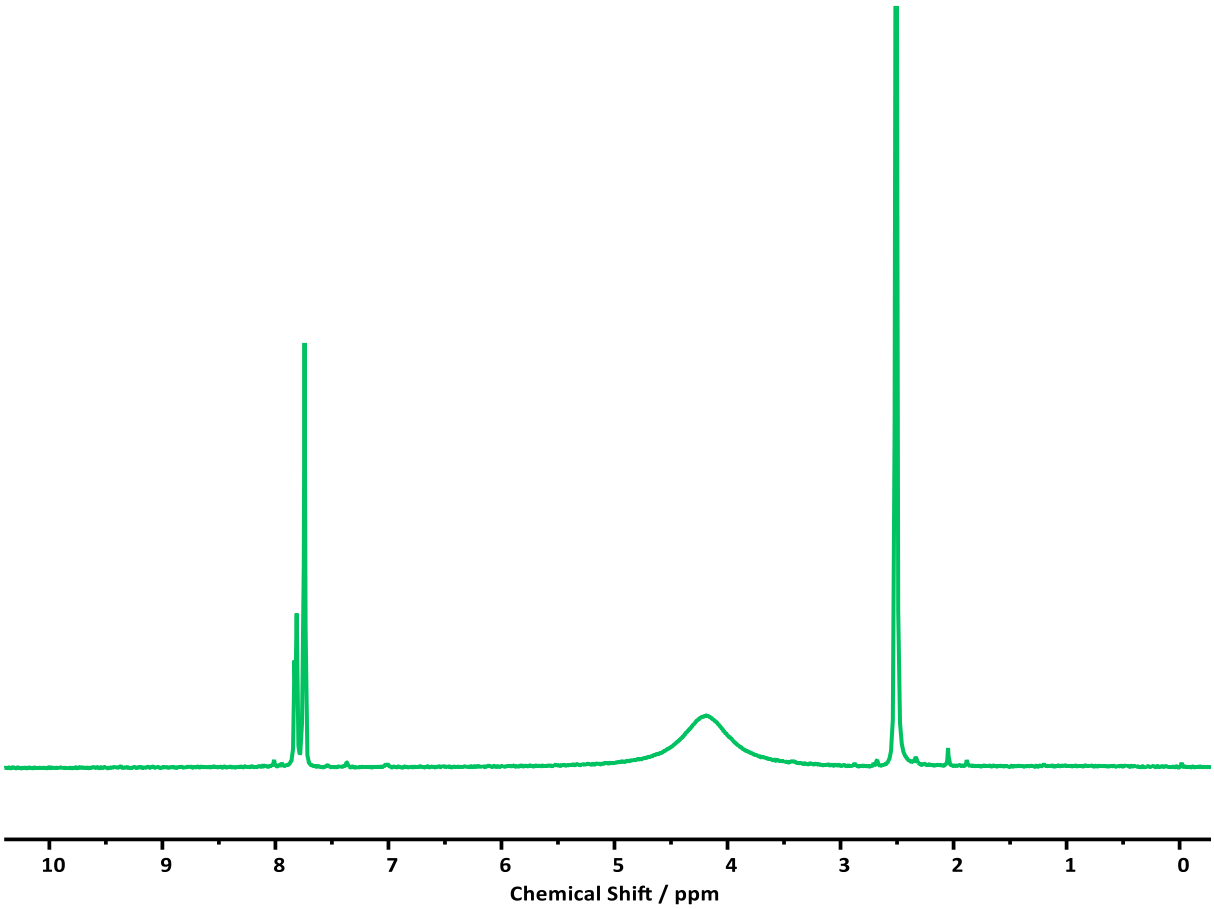

Figure S19. ^{1}H NMR spectrum of digested Cu(N_3-BDC) nanosheets, indicating desolvation of coordinated DMF by exfoliation in acetonitrile.

S4. Post-Exfoliation Functionalisation Data

S4.1. Experimental Conditions

Table S3. Experimental conditions for the click reactions performed using Cu(N_3-BDC) nanosheets.

	Cu(BDC-trz-CO_2H)	**Cu(BDC-trz-NMe_2)**	**Cu(BDC-trz-OH)**	**Cu(BDC-trz-Pyr)**
Cu(I)PF_6(MeCN)$_4$ / mg	15			
Acetylene derivative / mmol	0.04 (4 eq.)	0.40 (50 eq.)	1.00 (100 eq.)	(20 eq.)
Acetylene derivative / mg	2.80	33.3	70.1	45.2
Acetylene derivative / µL	3	55	75	-

S4.2. Characterisation of the Functionalised MONs

Due to the small quantity of MONs obtained from each experiment, some ^{1}H NMR spectra and PXRD patterns have poor signal to noise ratios.

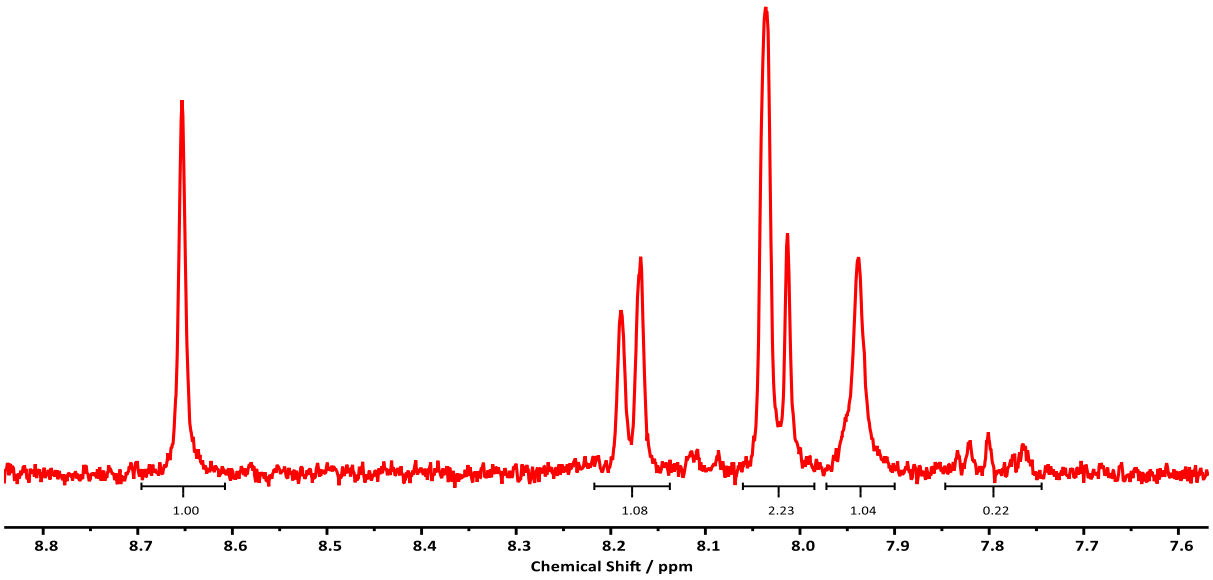

Figure S20. ^{1}H NMR spectrum of digested Cu(BDC-trz-CO_2H) MONs.

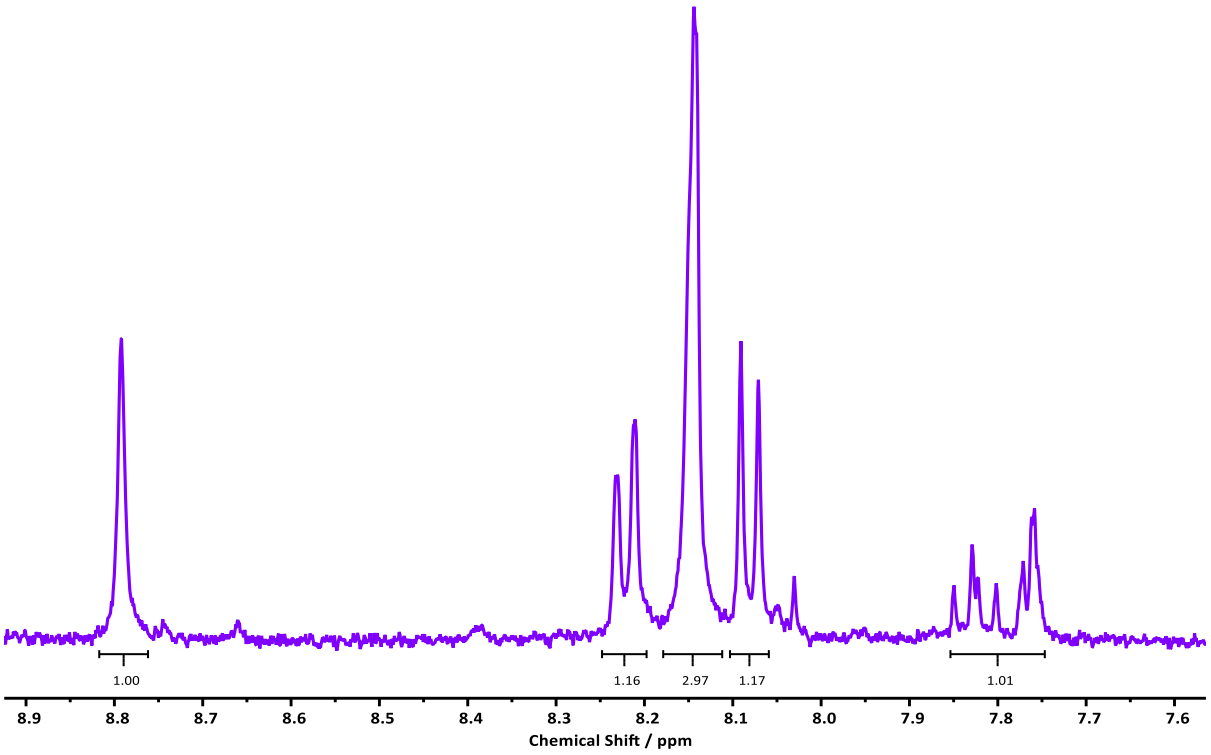

Figure S21. ^{1}H NMR spectrum of digested Cu(BDC-trz-NMe_2) MONs.

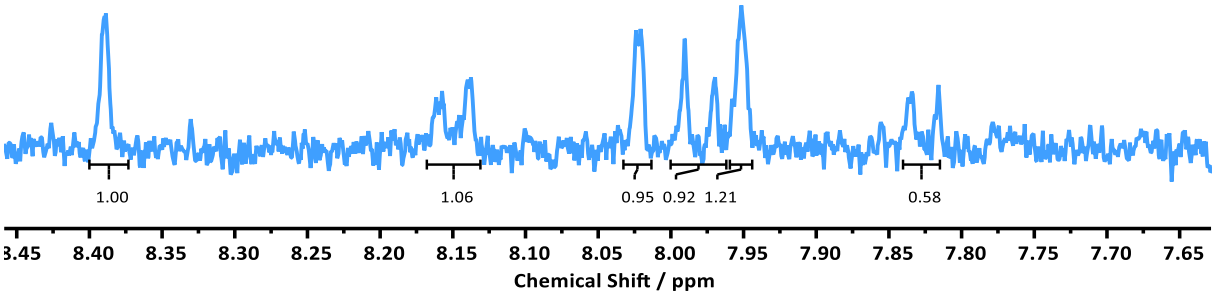

Figure S22. ^{1}H NMR spectrum of digested Cu(BDC-trz-OH) MONs.

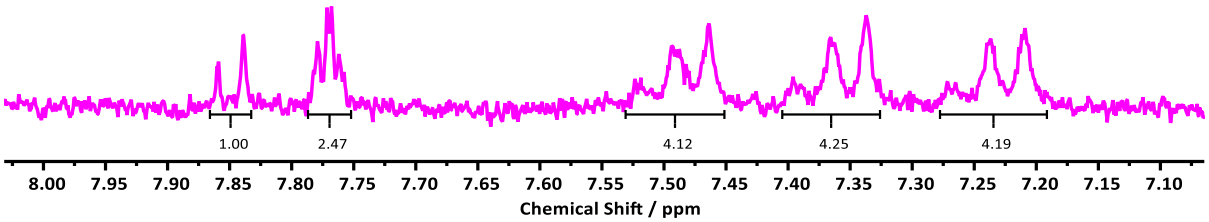

Figure S23. ^{1}H NMR spectrum of digested Cu(BDC-trz-pyr) MONs.

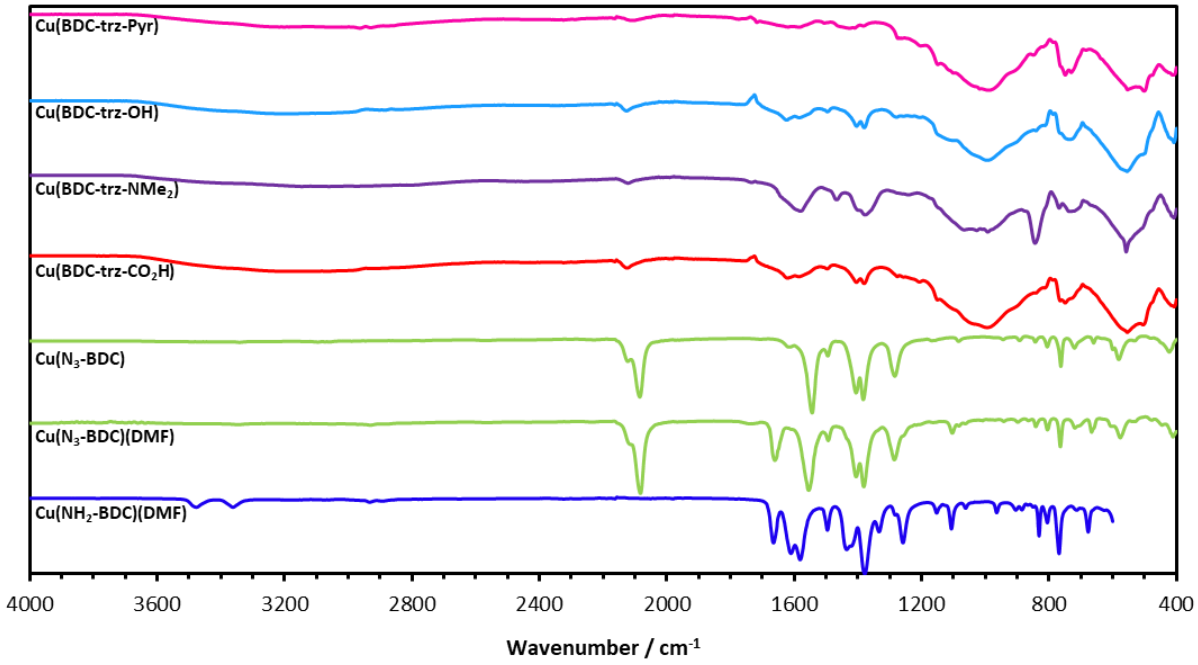

Figure S24. From bottom to top, FT-IR Spectra of: Cu(NH_2-BDC)(DMF) (dark blue), Cu(N_3-BDC)(DMF), desolvated Cu(N_3-BDC) (green), Cu(BDC-trz-CO_2H) nanosheets (red), Cu(BDC-trz-NMe_2) nanosheets (purple), Cu(BDC-trz-OH) nanosheets (light blue), and Cu(BDC-trz-pyr) nanosheets (pink).

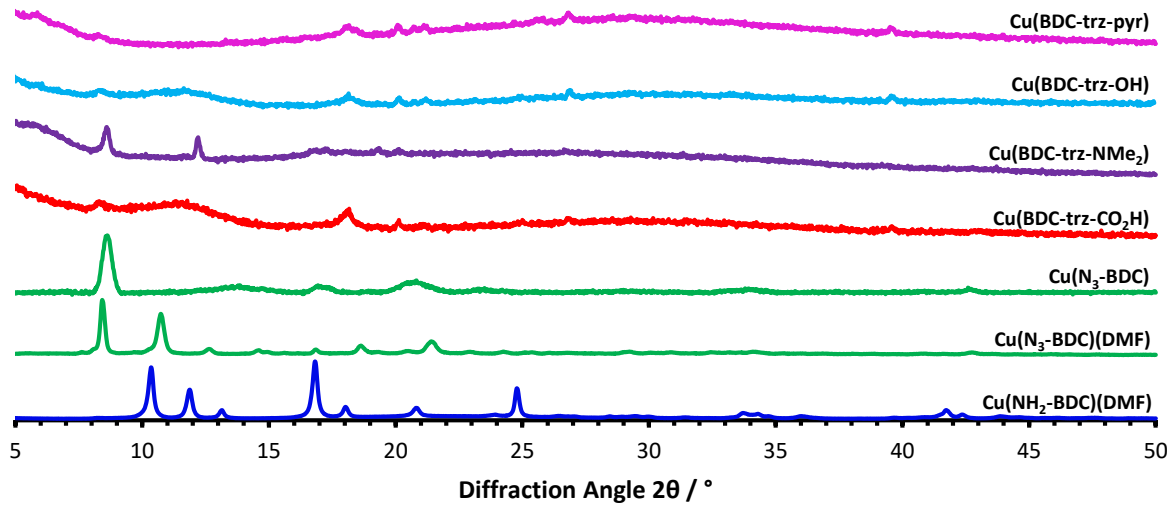

Figure S25. From bottom to top, X-ray powder diffraction patterns of: Cu(NH_2-BDC)(DMF) (dark blue), Cu(N_3-BDC)(DMF), desolvated Cu(N_3-BDC) (green), Cu(BDC-trz-CO_2H) nanosheets (red), Cu(BDC-trz-NMe_2) nanosheets (purple), Cu(BDC-trz-OH) nanosheets (light blue), and Cu(BDC-trz-pyr) nanosheets (pink).

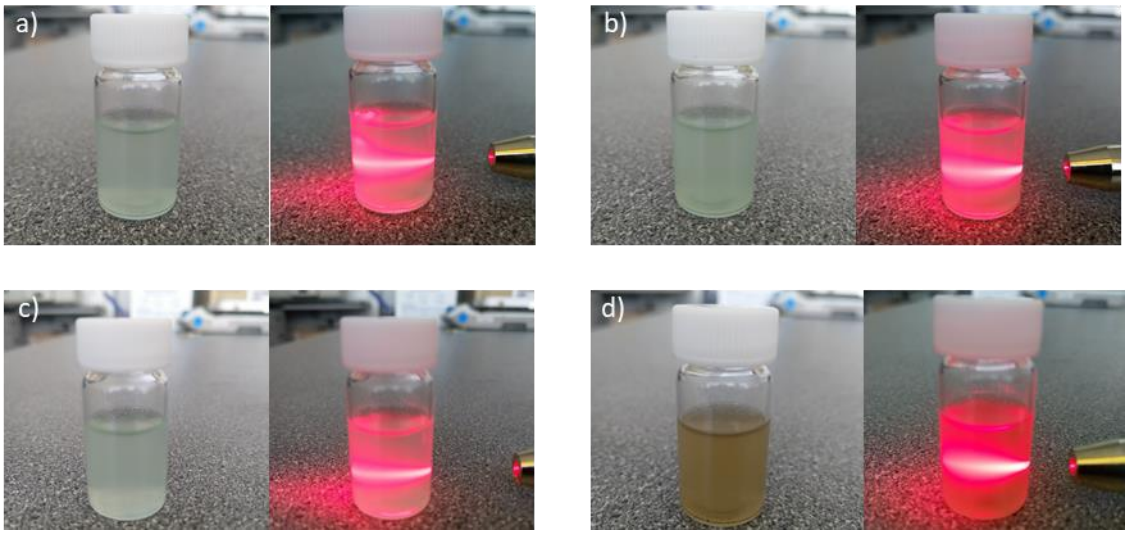

Figure S26. Images showing suspensions and associated Tyndall scattering of **a)** Cu(BDC-trz-CO_2H), **b)** Cu(BDC-trz-NMe_2), **c)** Cu(BDC-trz-OH), and **d)** Cu(BDC-trz-pyr) nanosheets.

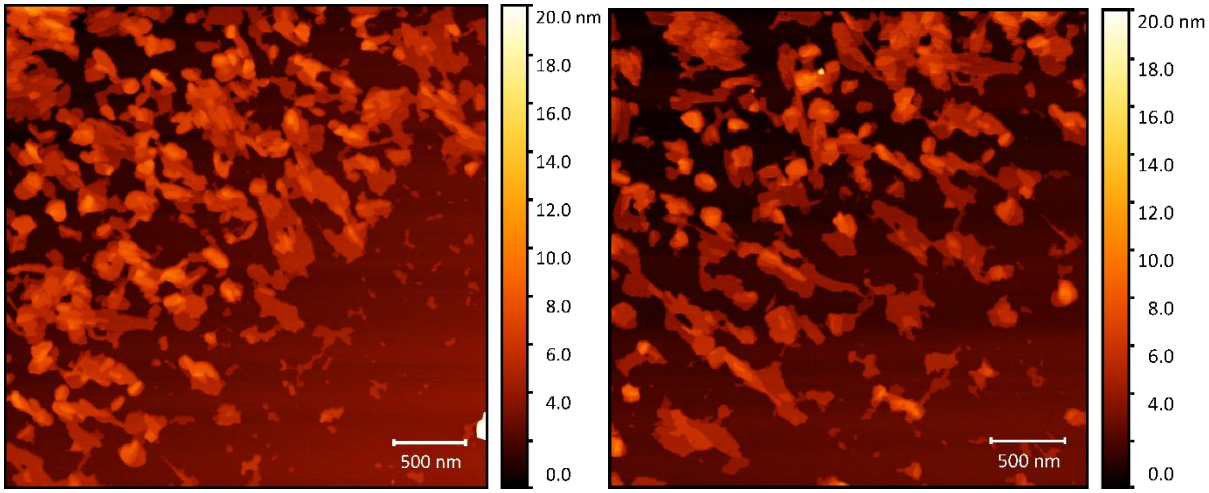

Figure S27. Additional AFM images of Cu(BDC-trz-CO_2H) nanosheets.

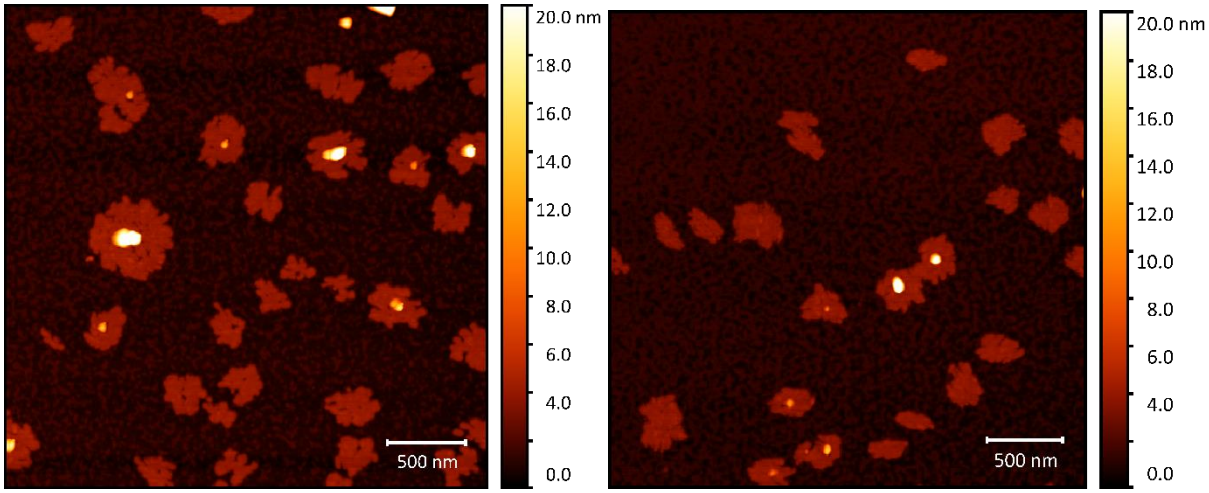

Figure S28. Additional AFM images of Cu(BDC-trz-NMe_2) nanosheets.

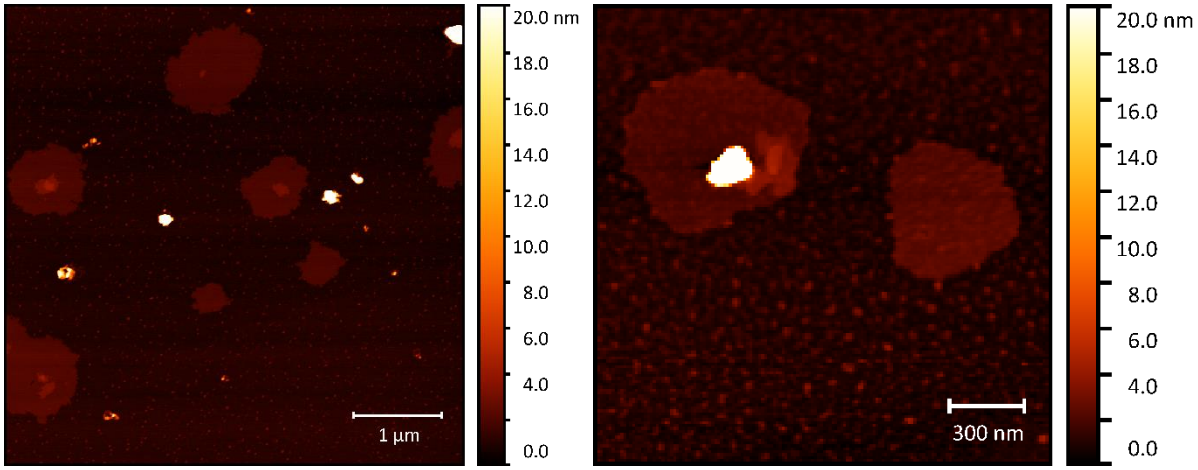

Figure S29. Additional AFM images of Cu(BDC-trz-OH) nanosheets.

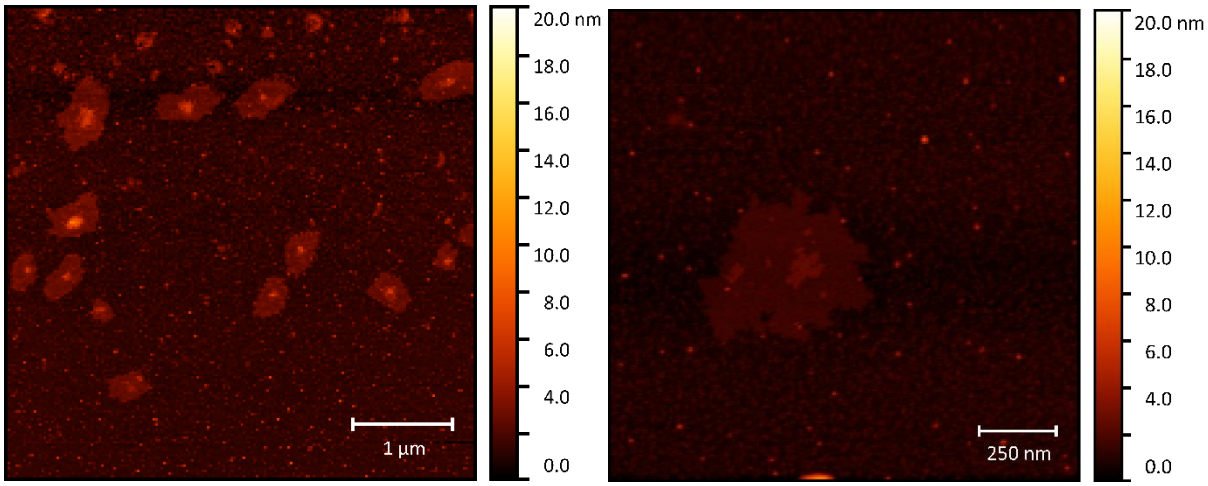

Figure S30. Additional AFM images of Cu(BDC-trz-pyr) nanosheets.

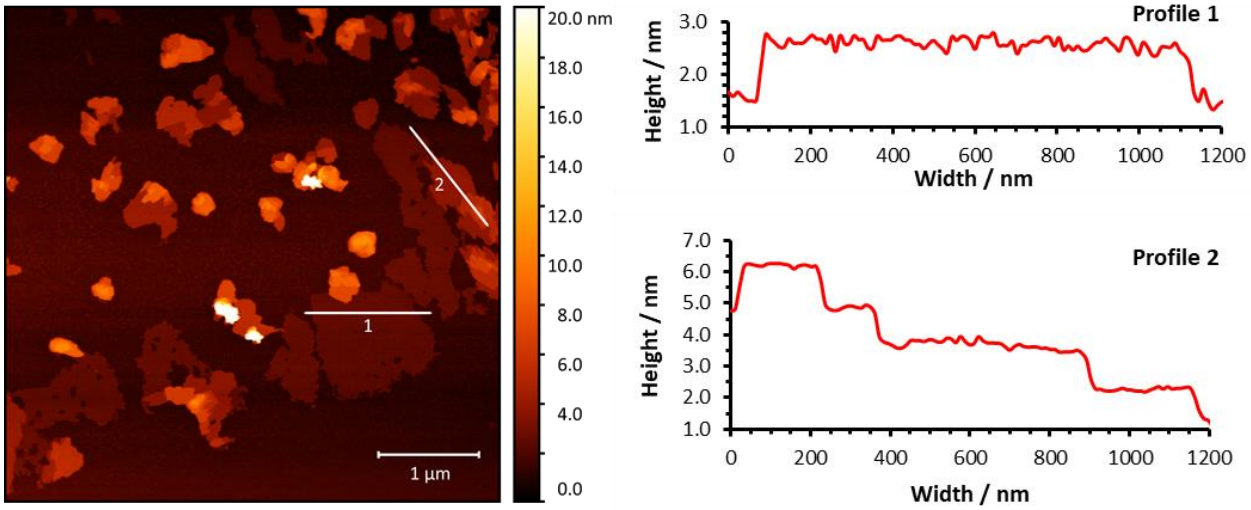

Figure S31. Height profiles for selected nanosheets shown in Figure 3a, for Cu(BDC-trz-CO_2H) nanosheets.

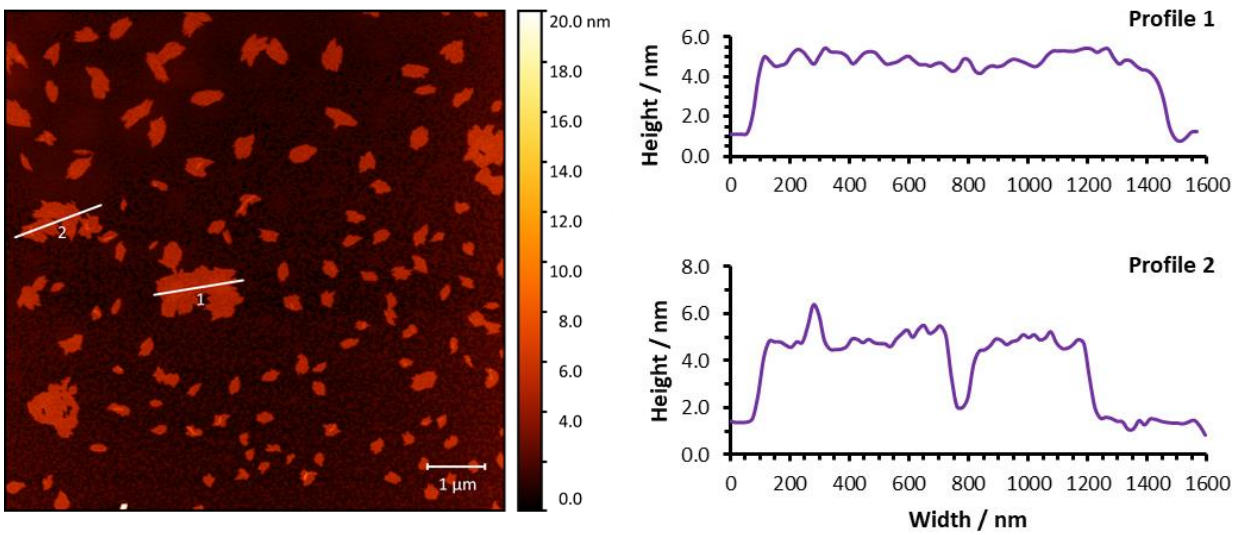

Figure S32. Height profiles for selected nanosheets shown in Figure 3b, for Cu(BDC-trz-NMe_2) nanosheets.

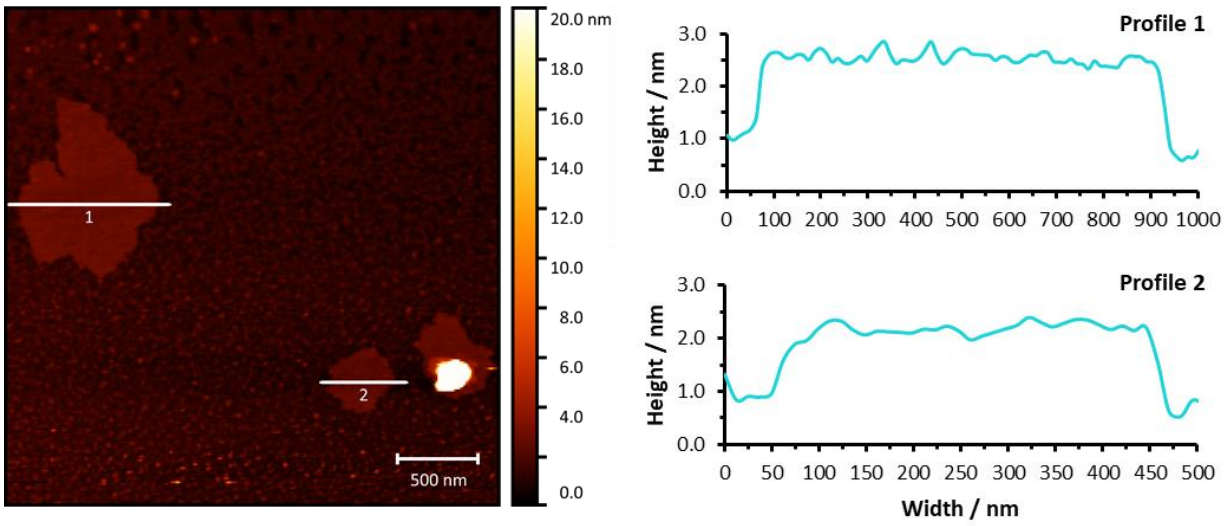

Figure S33. Height profiles for selected nanosheets shown in Figure 3c, for Cu(BDC-trz-OH) nanosheets.

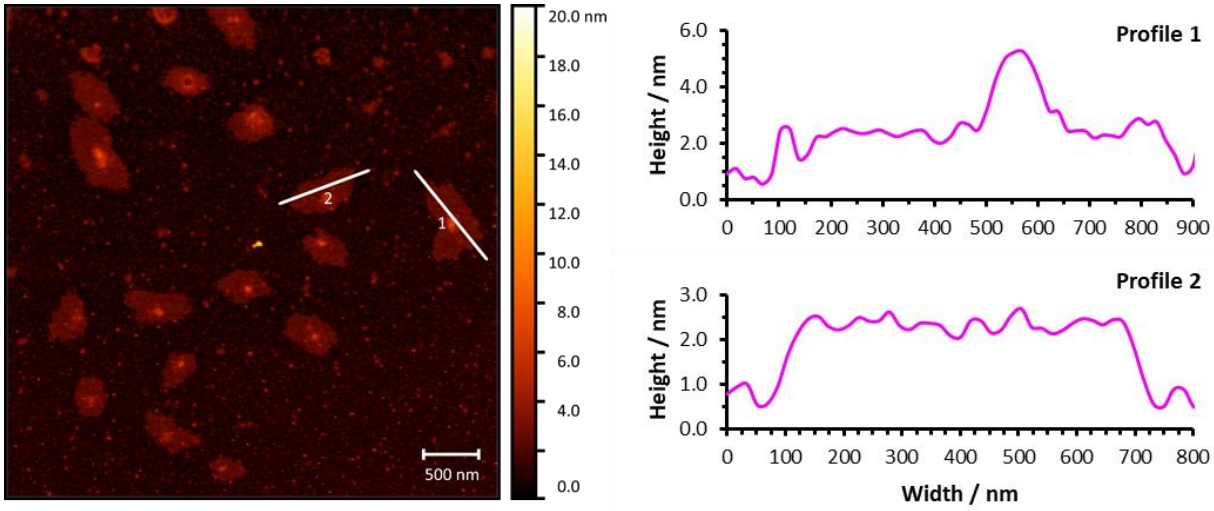

Figure S34. Height profiles for selected nanosheets shown in Figure 3d, for Cu(BDC-trz-pyr) nanosheets.

Table S4. Surface roughness values calculated for nanosheets shown in Figures S11 and S31-34.

Roughness	Cu(BDC-N_3)	Cu(BDC-trz-CO_2H)	Cu(BDC-trz-NMe_2)	Cu(BDC-trz-OH)	Cu(BDC-trz-Pyr)
Average, Ra / pm	57.9	41.2	116.6	52.2	221.6
Root mean square, Rq / pm	70.6	49.9	147.0	65.4	277.0

S5. Sensing

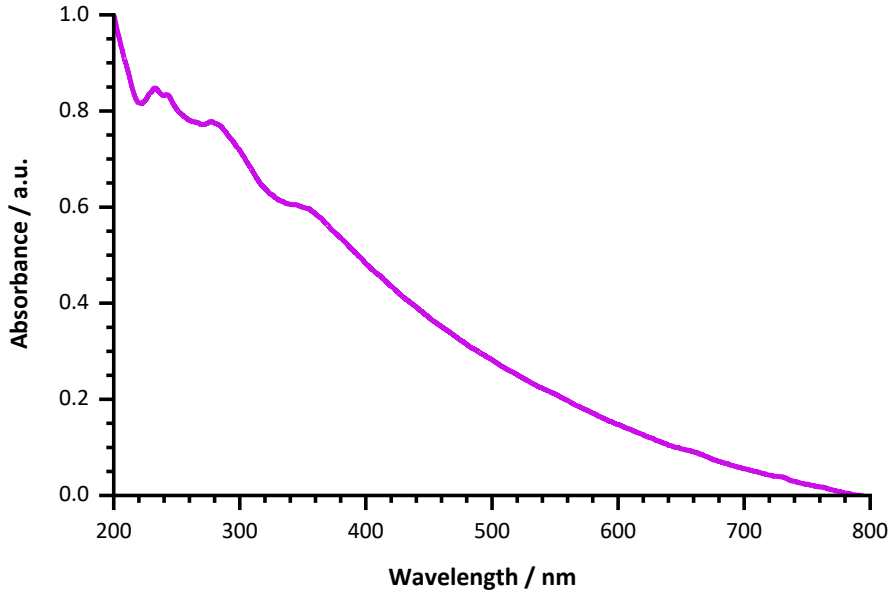

Figure S35. UV-Vis absorption spectrum of Cu(BDC-trz-pyr) nanosheets suspended in acetonitrile (0.1 mg mL^{-1}).

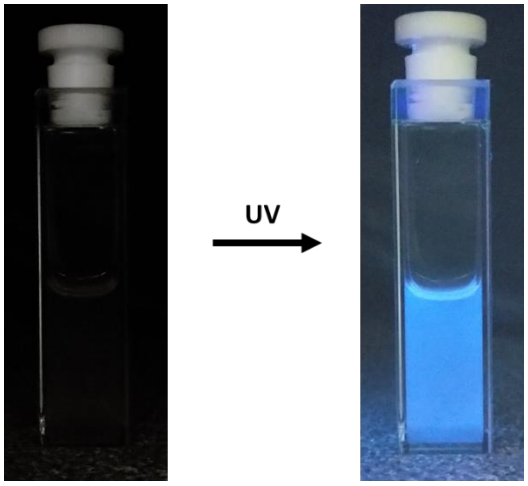

Figure S36. Images of the as prepared Cu(BDC-trz-pyr) nanosheets in acetonitrile before and after application of UV light.

S6. References

1 J. Nicks, J. Zhang and J. A. Foster, Tandem catalysis by ultrathin metal–organic nanosheets formed through post-synthetic functionalisation of a layered framework, *Chem. Commun.*, 2019, **55**, 8788–8791.

2 M. E. Braun, C. D. Steffek, J. Kim, P. G. Rasmussen and O. M. Yaghi, 1,4-Benzenedicarboxylate derivatives as links in the design of paddle-wheel units and metal – organic frameworks, *Chem. Commun. (Camb).*, 2001, **2**, 2532–2533.